A SPECTRAL VOLUME INTEGRAL EQUATION METHOD FOR ARBITRARY BI-PERIODIC GRATINGS WITH EXPLICIT FOURIER FACTORIZATION

M. C. van Beurden[*]

Eindhoven University of Technology, Den Dolech 2, 5612 AZ Eindhoven, The Netherlands

Abstract—For dielectric periodic gratings, we propose the combination of a spectral-domain volume integral equation and Fourier factorization rules to address the Gibbs phenomenon caused by jumps in both the fields and the permittivity. From a theoretical point of view we discuss two ways to overcome the computational complexity caused by the inverse rule by changing the fundamental unknowns of the underlying electromagnetic problem. The resulting numerical system is solved iteratively and the corresponding matrix-vector product has an $O(NM \log M)$ complexity, where M is the number of Fourier modes and N is the number of sample points in the longitudinal direction.

1. INTRODUCTION

Several powerful numerical methods to study scattering by periodic dielectric media are based on expansions in terms of Fourier series in the directions of periodicity, which lead to a natural decomposition of the Maxwell equations. The most well-known are the rigorous coupled wave analysis (RCWA) and the differential method. In spite of the natural decomposition, the performance of these methods was historically plagued by poor performance when arbitrarily polarized fields were considered in combination with piecewise homogeneous grating profiles. The matter was eventually resolved by the motivation and subsequent consistent derivation of the Fourier factorization rules [1–3], which gave rise to field-material interaction matrices that consist of proper combinations of the Laurent rule and the inverse rule. In turn, the Fourier factorization rules led to another approach,

originally defined for the differential method, based on the selection
of the continuous components of the electric field and flux densities,
via the definition of normal-vector fields at material boundaries and
the subsequent continuation of these fields to the entire body of the
grating profile [4]. Both methods have been combined successfully with
RCWA [3, 5].

Here, we discuss the impact of both Fourier factorization methods
on the efficiency and accuracy of the volume integral method,
formulated in the (transverse) spectral domain. Although the volume
integral method leads to a full three-dimensional problem that needs
to be solved as a whole, as opposed to the modular approach of
RCWA, the special structure and the bounded nature of the integral
operators have the potential to lead to an efficient numerical scheme
by employing iterative techniques in combination with an efficient
matrix-vector product. In principle, the volume integral method can
be formulated both in the spatial domain [6, 7] or in the (transverse)
spectral domain [8, 9]. For the spatial-domain formulation, a critical
issue is to efficiently compute the Green's function in terms of double-
infinite series, which can be handled via the Ewald transformation.
In the spectral domain, the Green's function is directly and efficiently
available per Fourier mode but now the field-material interactions need
careful attention, in view of the Fourier factorization rules that have
become so widespread in RCWA and the differential method. For two-
dimensional setups with one-dimensional periodicity, the use of the
normal-vector-field framework in combination with a volume-integral
equation was proposed in [10] and approximate Fourier factorization
rules for the three-dimensional case were employed in [9]. However,
in both cases no special attention was paid to the complexity of the
field-material interactions that arise due to the inverse rule, which
requires a matrix inverse that is defined across all the Fourier modes
involved. The direct consequence of the inverse rule is that the
efficiency deteriorates rapidly for an increasing number of Fourier
modes. It is the aim of the present paper to discuss measures to
overcome this computational bottleneck by reformulating the volume
integral method such that the effect of the inverse rule is taken into
account without suffering the consequences of the increase in the
asymptotic computational complexity of the rule and generalize the
work presented in [11], where an explicit Fourier factorization approach
was presented for the simplified setup of block-shaped gratings.

The paper is organized as follows. After a short introduction
to the volume integral method, Li's approach is reformulated in
terms of the volume integral method while keeping track of the
computational complexity. It is shown theoretically that this can lead

to an increase in the size of the numerical system in case of complicated grating geometries. Subsequently, the normal-vector-field formulation is considered and it is shown that this approach does not lead to an increase of the size of the linear system. The combination of the volume integral method and the normal-vector field approach is then demonstrated numerically.

2. THE VOLUME INTEGRAL METHOD

The volume integral equation method (VIM) for the time-harmonic solution, using the $\exp(j\omega t)$ time convention, of Maxwell's equations consists of two parts. The first one is an infinite set of integral representations, one for each Fourier mode, that describe a Fourier component of the total electric field $\mathbf{e}(m_1, m_2, z)$ in terms of the Fourier component of the incident field $\mathbf{e}^i(m_1, m_2, z)$ and the Fourier component of the contrast current density $\mathbf{j}(m_1, m_2, z')$, where the latter interacts with the Green's function $\overline{\overline{G}}(m_1, m_2, z, z')$, viz

$$\mathbf{e}^i(m_1, m_2, z) = \mathbf{e}(m_1, m_2, z) - \int\limits_{z' \in \mathbb{R}} \overline{\overline{G}}(m_1, m_2, z, z')\mathbf{j}(m_1, m_2, z')dz', \quad (1)$$

where m_1, $m_2 \in \mathbb{Z}$ denote the index of the pertaining Fourier mode. The Green's functions is defined for a planarly stratified medium in the z direction. A more detailed discussion on the Green's function is presented in [9, 11].

The second part to arrive at the volume integral method is formed by the field-material interactions that establish the relation between the contrast current density and the total electric field. This relation is most suitably formulated in the spatial domain as

$$\mathbf{J}(x, y, z) = j\omega \left[\varepsilon(x, y, z) - \varepsilon_b(z)\right] \mathbf{E}(x, y, z) = j\omega\chi(x, y, z)\mathbf{E}(x, y, z), \quad (2)$$

where $\mathbf{J}$ denotes the contrast current density, ω is the angular frequency, $\varepsilon(x, y, z)$ is the permittivity of the configuration, $\varepsilon_b(z)$ is the permittivity of the stratified background, and $\mathbf{E}$ denotes the total electric field. The transformation of the latter equation to a an approximation in finite Fourier series in the xy plane is the main focus here. For simplicity, we will assume that the Fourier series comprises a number of modes that is symmetrical and identical in the x and y direction, with upper and lower index $\pm M$.

A straightforward approach is to transform Equation (2) directly to the spectral domain

$$\mathbf{j}(m_1, m_2, z) = \sum_{k=-M}^{M} \sum_{\ell=-M}^{M} \chi_s(m_1 - k, m_2 - \ell, z)\mathbf{e}(k, \ell, z), \quad (3)$$

which amounts to a discrete convolution, also known as the Laurent rule. Further, $\chi_s(k, l, z)$ are the Fourier coefficients of the contrast function $\chi(x, y, z)$ with respect to the transverse (xy) plane. However, one of the major numerical issues in dealing with field-material interactions in a spectral basis is the observation that a simple product equation in real space is not always accurately reproduced by a convolution in Fourier space if one or both representations of the product variables have a finite (or truncated) Fourier expansion (as is the case in numerical implementations). In more detail, it has been shown that if both variables of the product satisfy a so-called concurrent complementary jump condition, then the "inverse rule" [1] has much better accuracy properties than the Laurent rule, which is the standard convolution for the truncated Fourier expansions. This observation has been worked out in full detail for 2D and 3D field-material interactions and given a solid theoretical foundation by Li [2, 3], within the context of RCWA.

For the volume integral method in the spectral domain, these observations are equally relevant since we employ a spectral discretization of the electric field and the contrast current density. Although the jumps in $\mathbf{E}$ and the contrast function are concurrent, they are *not* complementary, since the contrast function is zero outside the support of the perturbing geometry with respect to the background. Therefore, the rationale of Li's rules needs careful consideration. A second issue within the volume integral method is the efficiency of the inverse rule. Whereas the Laurent rule has a low computational complexity as a matrix-vector product, owing to implementations via FFTs, the inverse rule typically leads to a full-complexity matrix-vector product, which seriously degrades the efficiency of the method.

2.1. Cartesian Rules on a Tensor Grid

We consider the case of isotropic media for a binary grating in a homogeneous isotropic background layer with permittivity ε_b. Then the Li rules require modifications only for the field components in the transverse plane, i.e., the xy plane, since the electric-field component in the z direction is then continuous everywhere. We build the permittivity function on a tensor grid, i.e., out of a number of aligned blocks, which may or may not be adjacent. For a circular cross section, a possible approximation on a tensor grid is show in Figure 1. In particular, we write the permittivity function and the corresponding
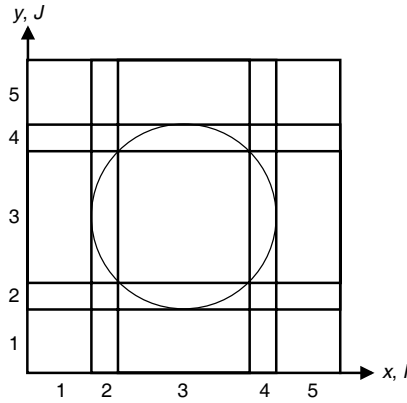
Figure 1. Circular geometry captured on a tensor grid.

inverse permittivity function as

$$\varepsilon(x,y) = \varepsilon_b \left[1 + \sum_{i=1}^{I} \sum_{j=1}^{J} \chi_{i,j} \Pi_i^x(x) \Pi_j^y(y) \right], \tag{4}$$

$$\varepsilon^{-1} = \varepsilon_b^{-1} \left[1 + \sum_{i=1}^{I} \sum_{j=1}^{J} \hat{\chi}_{i,j} \Pi_i^x(x) \Pi_j^y(y) \right], \tag{5}$$

where Π_α^β is a pulse function in the direction $\beta \in \{x, y\}$ with support on the full interval associated with the label α. In the x direction, there are I intervals and in the y direction there are J intervals. Further, $\chi_{i,j}$ are constants or continuous scalar functions on the support of the function $\Pi_i^x(x)\Pi_j^y(y)$, and $\hat{\chi}_{i,j} = -\chi_{i,j}/(1 + \chi_{i,j})$.

From the relation $E_x = \varepsilon^{-1} D_x$ for the x components of the electric field and flux, we obtain

$$E_x = \varepsilon_b^{-1} \left[1 + \sum_{i=1}^{I} \sum_{j=1}^{J} \hat{\chi}_{i,j} \Pi_i^x(x) \Pi_j^y(y) \right] D_x, \tag{6}$$

where, according to Li's line of reasoning [2, 3], $\Pi_i^x D_x$ is factorizable in Fourier space, but $\Pi_j^y D_x$ is not. Since the pulse functions Π_α^β can be interpreted as projection operators, we can employ the following.

Let I be the identity operator and A_i be a sequence of bounded operators that commute with the mutually orthogonal projection operators P_i, then the operator $1 + \sum_{i=1}^{I} A_i P_i$ has a bounded inverse

of the form $1 + \sum_{i=1}^{I} B_i P_i$, where $B_i = -A_i(1 + A_i)^{-1}$. The proof follows by working out the algebra and taking into account the idempotency of the projection operators.

With this result, we can now express the electric flux component in terms of electric-field component as

$$D_x = \varepsilon_b \left[1 - \sum_{i=1}^{I} \sum_{j=1}^{J} \hat{\chi}_{i,j} \Pi_i^x(x) \Pi_j^y(y) \left(1 + \sum_{k=1}^{I} \hat{\chi}_{k,j} \Pi_k^x(x) \right)^{-1} \right] E_x, \quad (7)$$

where the commutation property of A_i and B_i with P_i has been used.

Analogously, we have for the y components

$$D_y = \varepsilon_b \left[1 - \sum_{i=1}^{I} \sum_{j=1}^{J} \hat{\chi}_{i,j} \Pi_i^x(x) \Pi_j^y(y) \left(1 + \sum_{\ell=1}^{J} \hat{\chi}_{i,\ell} \Pi_\ell^y(y) \right)^{-1} \right] E_y. \quad (8)$$

Now each of the multiplication operators are Fourier factorizable after the inverse operations that operate directly on the components of the electric field have been performed. From these relations, we can derive the contrast current density in the usual way. The transformation of the above formulas to the spectral domain is now readily obtained by replacing the direct multiplication operators by the Laurent rule, which has a Toeplitz-matrix representation, and the inverses of the operator combinations by the "inverse rule", i.e., the inverse of a Toeplitz matrix. As a final step, we note that the contrast current density is then obtained by subtracting the electric flux density and the electric field, i.e.,

$$\mathbf{J} = j\omega(\mathbf{D} - \varepsilon_b \mathbf{E}). \quad (9)$$

From the above relations it becomes clear that every interval along the x and y direction gives rise to an inverse operator, i.e., a total of $I + J$ inverses. Each of these inverses can be avoided if we introduce auxiliary variables (vector fields) and corresponding linear equations to the matrix-vector product, to simultaneously solve both the volume integral equation, the field-material interaction relations, and the relations between the electric field $\mathbf{e}$ and the auxiliary variables grouped in $\mathbf{f}$, i.e., we can write

$$\begin{pmatrix} I & -G & 0 \\ I^r & 0 & C_1 \\ 0 & I^r & C_2 \end{pmatrix} \begin{pmatrix} \mathbf{e} \\ \mathbf{j} \\ \mathbf{f} \end{pmatrix} = \begin{pmatrix} \mathbf{e}^i \\ 0 \\ 0 \end{pmatrix}, \quad (10)$$

where I denotes the identity matrix and G represents the Green's function matrix per Fourier mode, as in Equation (1). Further I^r

is a matrix that repeats the identity matrix several times over its rows in blocks, C_1 represent the sequence of operators $(1 + \sum_{k=1}^{I} \hat{\chi}_{k,j} \Pi_k^x(x))$ or $(1 + \sum_{\ell=1}^{J} \hat{\chi}_{i,\ell} \Pi_\ell^y(y))$ whose inverse in Equations (7) and (8) was to be avoided, and C_2 represents the remaining sum of projection operators in Equations (7) and (8). Note that each of the operators forming C_1 or C_2 can be represented as a Toeplitz matrix (C_1) or a block-Toeplitz matrix (C_2) and therefore each corresponding matrix-vector product can be executed via one-dimensional or two-dimensional FFTs, respectively.

Hence, we preserve the efficiency of the matrix-vector product in the form of FFTs, at the expense of a larger set of variables and a dependence on the geometrical approximation of the scattering structure. This is especially the case if I and J are larger than one, since each of the inverses increases the number of auxiliary variables, thereby increasing the size of the total matrix-vector product and thereby increased the total computational complexity. In Appendix A, a (non-unique) way of avoiding an unlimited number of inverses is discussed, thereby restricting the number of unknowns to at most three times the number of unknowns present in the electric field. The case for a single rectangular pilar or hole ($I = J = 1$), for which there is no increase in the computational complexity, is discussed and demonstrated in [11].

Another approach to reduce the complexity of the inverses appearing in Equations (7) and (8) is to exploit the structure of the inverse of a Toeplitz matrix in the form of the Gohberg-Semencul and Gohberg-Heinig formulas, see, e.g., [12]. The disadvantage of such an approach is that additional preprocessing is needed and that the computational complexity of the matrix-vector product for the inverse Toeplitz matrix is at least three times larger than that for a single Toeplitz matrix.

2.2. Normal-vector Field Formulation

The discussion of the Cartesian rules above shows that field-material interactions of low computational complexity, via FFTs, depend on the type of geometry of the contrast function, since a complicated geometry leads to an increase in the total number of unknowns, even when the ideas of Appendix A are taken into account. Therefore, it is preferable to operate in a framework in which FFTs remain the dominant operation of the field-material interaction equations and in which the number of unknowns is kept to a minimum. The framework

first proposed in [4] offers exactly this. The key idea put forward there, is the construction of an auxiliary vector field $\mathbf{F}$ that is continuous everywhere, with the possible exception of isolated points or lines that correspond to edges and corners in the geometry of the permittivity function. The continuous vector field $\mathbf{F}$ is formed by the sum of electric-field components that are tangential to material boundaries and electric-flux-density components normal to material boundaries, with the help of a normal-vector field generated in a preprocessing step, see, e.g., [5, 13].

The most commonly employed field-material interaction formula used in the context of RCWA and the Differential Method is given by [4, Equation (15)]

$$\mathbf{D} = Q_\varepsilon \mathbf{E}, \tag{11}$$

which was also the starting point in [10] for an integral equation formulation for two-dimensional scattering. However, it is more interesting to go back to the relations between auxiliary field $\mathbf{F}$ and the electric field and flux density [4, Equations (12) and (13)]

$$\mathbf{E} = C_\varepsilon \mathbf{F}, \tag{12}$$
$$\mathbf{D} = \varepsilon C_\varepsilon \mathbf{F}. \tag{13}$$

From these relations, the contrast-current density can be written as

$$\mathbf{J} = j\omega \left[\varepsilon C_\varepsilon \cdot C_\varepsilon^{-1} - \varepsilon_b \right] \mathbf{E}. \tag{14}$$

Again we observe the presence of the inverse rule in the form of C_ε^{-1}, whereas the operators C_ε and $\varepsilon C_\varepsilon$ themselves have a representation in the spectral domain in the form of the (two-dimensional) Laurent rule, which we denote as c_ε and $\varepsilon c_\varepsilon$, respectively. However, as opposed to the Cartesian rules discussed above, there is only a single inverse present now and the idea of avoiding the inverse operations by introducing an auxiliary set of variables boils down to the formulation of the volume integral equation in terms of the auxiliary vector field $\mathbf{F}$ directly, i.e.,

$$\mathbf{e}^i(m_1, m_2, z) = (c_\varepsilon \mathbf{f})(m_1, m_2, z)$$
$$- \int_{z' \in \mathbb{R}} \overline{\overline{G}}(m_1, m_2, z, z') [(\varepsilon c_\varepsilon - \varepsilon_b \cdot c_\varepsilon) \mathbf{f}](m_1, m_2, z') dz', \tag{15}$$

where $\mathbf{f}$ is the spectral-domain counterpart of $\mathbf{F}$. By solving the linear system for the auxiliary variable $\mathbf{F}$, we maintain an efficient matrix-vector product for the above equation in the form of two-dimensional FFTs in the transverse plane, while taking into account the rationale of the Fourier factorization rules and without sacrificing additional memory for auxiliary variables. Further, the quantities that are usually derived from the electric field such as reflection and transmission coefficients, can now also be obtained from $\mathbf{F}$, owing to the operator C_ε that relates $\mathbf{F}$ to $\mathbf{E}$ and this requires no inverses to be computed.

3. NORMAL-VECTOR FIELD COEFFICIENTS FOR A BINARY GRATING

For a binary grating, i.e., a grating that has a uniform permittivity profile over its entire height, the volume-integral method requires the solution of the field $\mathbf{f}$ as given in Equation (15). For such a binary grating, the normal-vector field does not need to depend on the coordinate z and therefore also the coefficients of c_ε and $\varepsilon c_\varepsilon$ can be independent of z. This saves both memory and computation time, since the preprocessing step of generating the normal-vector field and the coefficients of c_ε and $\varepsilon c_\varepsilon$ are only needed for a single cross-section.

We consider a rectangular unit cell $x \in [-a/2, a/2]$, $y \in [-b/2, b/2]$ with isotropic materials, where the permittivity function of the binary grating is given by $\varepsilon(x, y)$. Further $n_x(x, y)$ and $n_y(x, y)$ are the x and y components of the generated normal-vector field. For this case, we have the following expressions for the coefficients of c_ε

$$\begin{pmatrix} e_x \\ e_y \\ e_z \end{pmatrix} = c_\varepsilon \mathbf{f} = \begin{pmatrix} c_{xn} & c_{xt} & 0 \\ c_{yn} & c_{yt} & 0 \\ 0 & 0 & I \end{pmatrix} \begin{pmatrix} f_n \\ f_t \\ f_z \end{pmatrix}, \quad (16)$$

where I represents the identity operator and the subscripts $_n$ and $_t$ denote the normal and tangential components, with respect to material boundaries. The coefficients of the convolution operators $c_{..}$ are given by

$$c_{xn}(m_1, m_2) = \frac{1}{ab} \int\limits_{-a/2}^{a/2} \int\limits_{-b/2}^{b/2} \frac{n_x(x, y)}{\varepsilon(x, y)} \exp\left[j\left(\mathbf{k}_T^m \cdot \mathbf{r}_T\right)\right] dy dx, \quad (17)$$

$$c_{yn}(m_1, m_2) = \frac{1}{ab} \int\limits_{-a/2}^{a/2} \int\limits_{-b/2}^{b/2} \frac{n_y(x, y)}{\varepsilon(x, y)} \exp\left[j\left(\mathbf{k}_T^m \cdot \mathbf{r}_T\right)\right] dy dx, \quad (18)$$

$$c_{xt}(m_1, m_2) = \frac{1}{ab} \int\limits_{-a/2}^{a/2} \int\limits_{-b/2}^{b/2} -n_y(x, y) \exp\left[j\left(\mathbf{k}_T^m \cdot \mathbf{r}_T\right)\right] dy dx, \quad (19)$$

$$c_{yt}(m_1, m_2) = \frac{1}{ab} \int\limits_{-a/2}^{a/2} \int\limits_{-b/2}^{b/2} n_x(x, y) \exp\left[j\left(\mathbf{k}_T^m \cdot \mathbf{r}_T\right)\right] dy dx, \quad (20)$$

where $\mathbf{k}_T^m$ are the reciprocal lattice vectors, depending on m_1 and m_2 and $\mathbf{r}_T = x\mathbf{u}_x + y\mathbf{u}_y$. The expressions for $\varepsilon c_\varepsilon$ are similar but now all

integrands are multiplied by $\varepsilon(x, y)$ and the remaining part of $\varepsilon c_\varepsilon$ that represents the mapping from f_z to e_z is given by

$$\varepsilon c_{\varepsilon, zz} = \frac{1}{ab} \int\limits_{-a/2}^{a/2} \int\limits_{-b/2}^{b/2} \varepsilon(x, y) \exp\left[j\left(\mathbf{k}_T^m \cdot \mathbf{r}_T\right)\right] dy dx. \qquad (21)$$

Note that in the above expressions, e_z and f_z are identical and the coupling between the z component and the transverse components of **e** and **f** is zero. This amounts to a significant saving in multiplications between Fourier coefficients and it saves one two-dimensional FFT, compared to the case of a general grating.

For the discretization of **f** in the z-direction, we employ a piece-wise linear approximation along the interval spanning the height of the grating, in combination with a collocation scheme. The semi-separability [14] of the Green's function kernels allows for a matrix-vector product, regarding the Green's functions only, with linear complexity, as further detailed in [15, Section 2D] and [10].

The computational advantages for a binary grating can be transferred to more general gratings by following the approach taken in RCWA, in which a grating is approximated by a stack of binary gratings. This means that we choose a sequence of disjoint intervals in the z direction and for each of these intervals we approximate the permittivity function by a permittivity function that is independent of the z direction. Then, by using a discretization in the z-direction for **f** that is dedicated to each of the intervals, we arrive at a sequence of binary gratings, for which we generate a two-dimensional normal-vector field and compute the coefficients of the field-material interaction operators.

4. NUMERICAL RESULTS

From the above discussion, it is clear that the most expedient implementation of the spectral-domain volume integral equation involves the normal-vector-field formulation, which is also the most flexible one in terms of curved material boundaries. To compare our results with results obtained with RCWA [5], an array of cavities with square cross section of edge length 0.5λ in a metal layer with relative permittivity $0.8125 - j \cdot 5.25$ and thickness 0.1λ, where λ is the wavelength of the normally incident plane wave in free space. The upper halfspace and the cavities have relative permittivity equal to 1, and the lower halfspace has a relative permittivity of 2.25. The periods in the x- and y-directions are equal to 2λ and the incident wave is polarized in the x direction. The volume integral equation
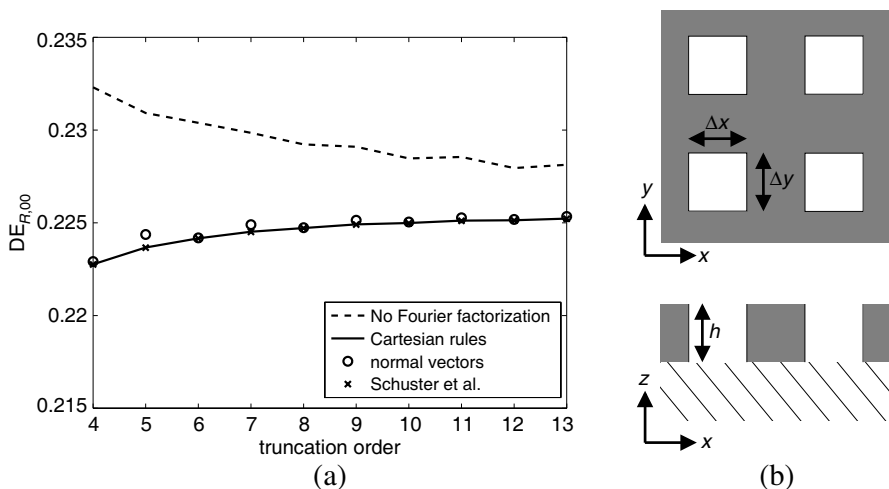
Figure 2. (a) Zeroth-order diffraction efficiency in reflection versus the truncation order in the Fourier modes for an array of cavities with (b) square cross section, compared to the results by Schuster et al. [5].

is combined with the Cartesian rules as discussed in Section 2.1 and with the normal-vector field with a piecewise-constant normal-vector field. Further, 33 samples in the z direction were used and the BiCGstab(2) [16] iterative solver without further preconditioning was employed to solve the linear system. Figure 2 shows the diffraction efficiency for the 0-th order reflection versus the truncation order, i.e., the upper index M of the Fourier modes in one periodic direction. As a reference, we repeat the results in [5], computed with RCWA for the piecewise-constant normal-vector field. We note that the Cartesian rules for a single square cavity leads to a formalism with the same number of unknowns as the normal-vector field formulation and therefore the approaches are of comparable complexity [11]. Also note that when the Fourier factorization rules are not taken into account, the convergence of the diffraction efficiency is much poorer, which is similar as for RCWA.

In Figure 3, the same setup is considered as before, but now for an array of holes with circular cross section with diameter equal to 0.5λ and the incident wave is diagonally polarized, i.e., $E_x = E_y$. Both the reference result and the result computed via the volume integral equation with the normal-vector fields have been obtained via a fully radial normal-vector field. For the volume integral equation, 33 linear expansion functions were used in the z-direction. Subsequent refinement in the z-direction did not further improve the convergence.

(a)   (b)
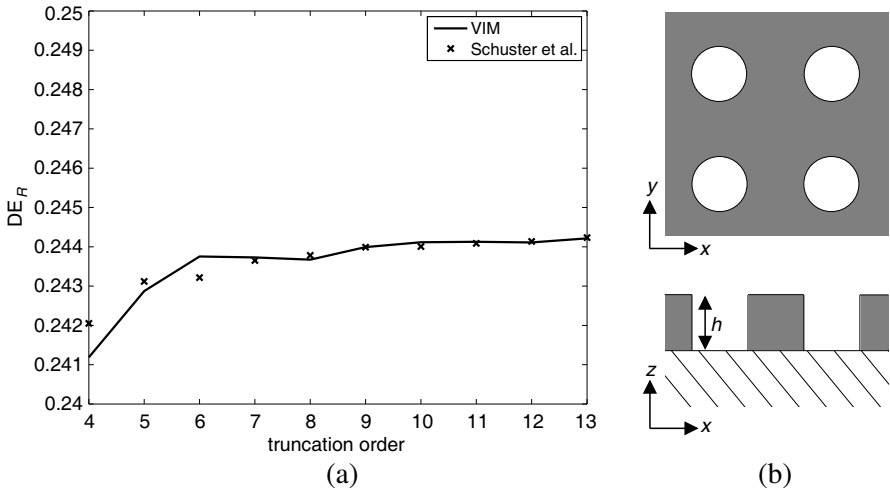
Figure 3. (a) Zeroth-order diffraction efficiency in reflection versus the truncation order in the Fourier modes for an array of cavities with (b) circular cross section, compared to the results by Schuster et al. [5].

(a)   (b)
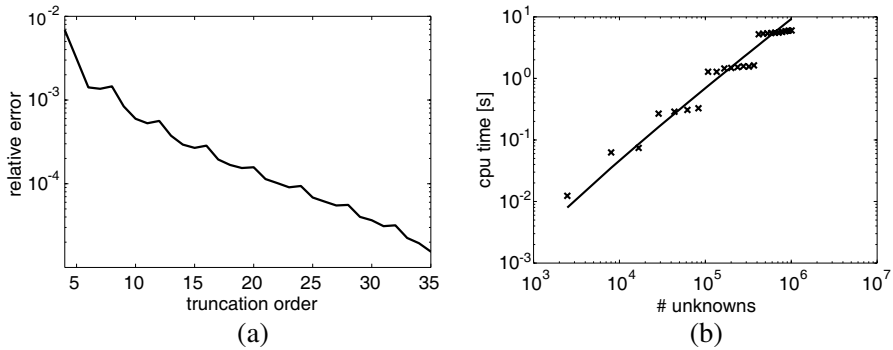
Figure 4. (a) Relative error versus the truncation order in the Fourier modes for an array of cavities with circular cross section. (b) CPU time per matrix-vector product versus total number of unknowns. The solid line is given by $\alpha N \cdot M \log(M)$, with M the total number of modes and N the number of samples in z. The solid line corresponds to the asymptotic complexity estimate of the matrix-vector product.

Good agreement between the results can be observed from this figure. To further investigate the convergence of the volume integral equation, we have increased the number of Fourier modes per direction to ± 50, i.e., a total number of 10201 Fourier modes in the transverse plane,

and the number of samples in the z-direction to 65. The result of this computation is used as a reference result for an increasing number of Fourier modes between ± 4 and ± 35 and 33 samples in z. The behavior of the corresponding relative error is shown in Figure 4. The corresponding cpu time per matrix-vector product is shown on the right-hand side of Figure 4 together with the complexity estimate of the matrix-vector product. The computations were performed on a Pentium M single-core laptop operating at a clock frequency of 1.86 GHz and with 1 GB RAM. As can be seen, the computation data exhibits several steps that correspond to steps in the FFT size.

Finally, to demonstrate the capabilities of the proposed approach for other practical applications, a stack of periodic structures is considered that exhibits a bandgap. The stack consists of layers with alternatingly aerial holes and solid pillars with circular cross section in air. The setup for one layer of holes and one layer of pillars is shown in Figure 5. This type of structure was inspired by the structure studied in [17], where a face-centered cubic lattice of partly overlapping holes was considered. The dimensions of the structure are summarized in Table 1. The material forming the pillars and the material surrounding the holes has permittivity $\varepsilon_r = 12.0$. A stack consisting of three layers with holes and three layers of pillars has been analyzed, where each combination of holes and pillars is shifted over one third of the period in the x direction. The zeroth order diffraction efficiency in transmission

(a)   (b)
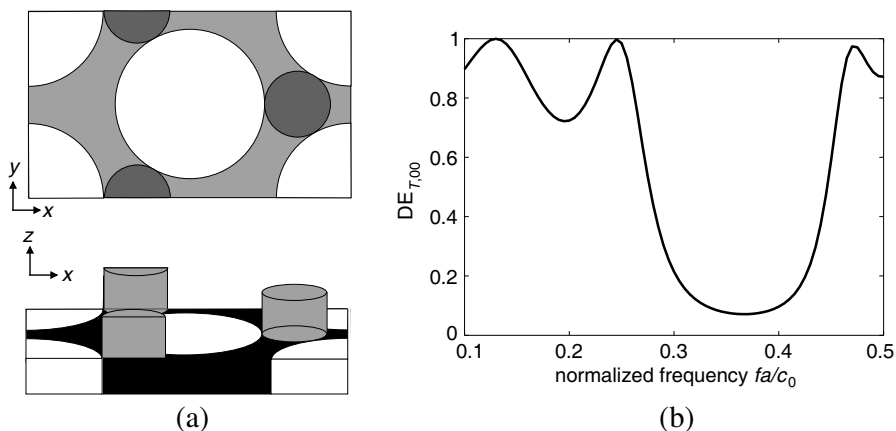
Figure 5. (a) Top and side view of a layer of pillars on top of a layer with holes in an face-centered cubical lattice. (b) Zeroth order diffraction coefficient in transmission for a configuration consisting of three layers of the structure on the left, each one shifted over one-third of a period in the x-direction.

Table 1. Dimensions of parameters of the structure of holes and pillars in Figure 5.

parameter	dimension
period in x-direction	$\sqrt{3}a$
period in y-direction	a
radius of the holes	$0.414a$
radius of the pillars	$0.162a$
height of the holes	$0.4a$
height of the pillars	$0.4a$

versus the normalized frequency fa/c_0, where $f = \omega/2\pi$, is shown in Figure 5. The bandgap behavior of this structure is clearly observed. The computations were performed using 15 Fourier modes in x and in y and eight sample points in the z-direction per layer of holes or pillars, i.e., a total of 48 sample points in the z-direction.

5. CONCLUSIONS

We have discussed a reformulation of the volume integral method for permittivity gratings in combination with the frameworks of the Fourier factorizations rules by Li and by Popov and Nevière, to deal with field-material interaction matrices that operate on a spectral basis. We have demonstrated how the asymptotic computational complexity of the inverse rule in the Fourier factorization rules can be effectively reduced to $O(NM \log M)$, where M is the number of Fourier modes and N the number of sample points in z. The proposed solution is to solve for a different but equivalent set of fundamental unknowns. The approach has been demonstrated by several numerical examples and has been validated against the results published in the literature.

APPENDIX A. REDUCING THE NUMBER OF INVERSE OPERATORS IN THE CARTESIAN RULES

The apparent observation in Section 2.1 is that each projection operator Π_α^β introduces a new auxiliary vector field, which makes this procedure rather inefficient for geometries that require more than a few projection operators. Therefore, we present a way to restrict this number to two auxiliary fields per direction. First, we observe that the inverse operators in Equations (7) and (8) only involve one

direction x or y, whereas the inverse rule in the normal-vector-field formulation is inherently two-dimensional. To make the inverses for the Cartesian rules two-dimensional, we note that the discontinuities in the projection operators are the ones giving rise to the inverse rule. If we can reduce the number of projection operators, we also reduce the number of inverse operators and thereby the number of auxiliary fields. At the same time, this means that the factors $\chi_{i,j}$ in Equation (4) need to become continuous functions of x and y, since otherwise jumps in these functions still need to be treated by the inverse rules. To separate the continuous from the discontinuous parts, we group the projection operators in alternating sequences, i.e., we introduce the even and odd projection operators

$$\Pi_o^x(x) = \sum_{k=1}^{I} \Pi_{2k-1}^x(x), \tag{A1}$$

$$\Pi_e^x(x) = \sum_{k=1}^{I} \Pi_{2k}^x(x), \tag{A2}$$

assuming that the unit cell is spanned by an even number of intervals I along the x direction. We introduce analogous projection operators along the y direction. The even and odd projection operators are mutually orthogonal, owing to their support. Since each rectangular area on the tensor grid is now part of the support of a unique product of the even and odd projection operators and each of the four possible products is takes the form of a sequence of non-connected areas with amplitude one, embedded in an area with amplitude zero, we can rewrite the inverse permittivity function as

$$
\begin{aligned}
\varepsilon^{-1} = \; & \varepsilon_b^{-1} \left[1 + f_{oo}(x,y)\Pi_o^x(x)\Pi_o^y(y) + f_{oe}(x,y)\Pi_o^x(x)\Pi_e^y(y) \right. \\
& \left. + f_{eo}(x,y)\Pi_e^x(x)\Pi_o^y(y) + f_{ee}(x,y)\Pi_e^x(x)\Pi_e^y(y) \right], \tag{A3}
\end{aligned}
$$

where each of the functions f_{ab}, $a, b \in \{e, o\}$, can be constructed as continuous functions owing to the isolation of the areas. The continuity of the functions can for instance be reached by using a linear interpolation between the supporting areas of the pertaining projection operator. Hence only four two-dimensional projection operators involved.

Following the method outlined in Section 2.1, we arrive at the following Fourier factorization rule

$$
\begin{aligned}
D_x = \; & \varepsilon_b \left\{ 1 - \left[f_{oo}(x,y)\Pi_o^y(y) + f_{oe}(x,y)\Pi_e^y(y) \right] \Pi_o^x(x) \right. \\
& \times \left[I + f_{oo}(x,y)\Pi_o^y(y) + f_{oe}(x,y)\Pi_e^y(y) \right]^{-1} \\
& - \left[f_{eo}(x,y)\Pi_o^y(y) + f_{ee}(x,y)\Pi_e^y(y) \right] \Pi_e^x(x) \\
& \left. \times \left[I + f_{eo}(x,y)\Pi_o^y(y) + f_{ee}(x,y)\Pi_e^y(y) \right]^{-1} \right\} E_x, \tag{A4}
\end{aligned}
$$

and a similar expression for the relation between D_y and E_y.

To finalize the procedure, we introduce two auxiliary fields $\mathbf{F}^e$ and $\mathbf{F}^o$, with x components satisfying

$$E_x(x,y) = \left[1 + f_{oo}(x,y)\Pi_o^y(y) + f_{oe}(x,y)\Pi_e^y(y)\right] F_x^o(x,y), \quad \text{(A5)}$$

$$E_x(x,y) = \left[1 + f_{eo}(x,y)\Pi_o^y(y) + f_{ee}(x,y)\Pi_e^y(y)\right] F_x^e(x,y), \quad \text{(A6)}$$

and similar relations for the y components. With these conditions, we finally obtain

$$\begin{aligned}
J_x = \; & \varepsilon_b \big\{ - \left[f_{oo}(x,y)\Pi_o^y(y) + f_{oe}(x,y)\Pi_e^y(y)\right] \Pi_o^x(x) F_x^o \\
& - \left[f_{eo}(x,y)\Pi_o^y(y) + f_{ee}(x,y)\Pi_e^y(y)\right] \Pi_e^x(x) F_x^e \big\}, \quad \text{(A7)}
\end{aligned}$$

and a similar relation for the y components. The operators linking $\mathbf{F}^{o,e}$ and $\mathbf{E}$ have a two-dimensional character, as opposed to the operators in Section 2.1. Nevertheless, all operators are now multiplication operators that have an efficient matrix-vector product implementation via two-dimensional FFTs.

REFERENCES

1. Lalanne, P. and G. M. Morris, "Highly improved convergence of the coupled-wave method for TM polarization," *J. Opt. Soc. Am. A*, Vol. 13, No. 4, 779–784, 1996.

2. Li, L., "Use of Fourier series in the analysis of discontinuous periodic structures," *J. Opt. Soc. Am. A*, Vol. 13, No. 9, 1870–1876, 1996.

3. Li, L., "New formulation of the Fourier modal method for crossed surface-relief gratings," *J. Opt. Soc. Am. A*, Vol. 14, No. 10, 2758–2767, 1997.

4. Popov, E. and M. Nevière, "Maxwell equations in Fourier space: Fast-converging formulation for diffraction by arbitrary shaped, periodic, anisotropic media," *J. Opt. Soc. Am. A*, Vol. 18, No. 11, 2886–2894, 2001.

5. Schuster, T., J. Ruoff, N. Kerwien, S. Rafler, and W. Osten, "Normal vector method for convergence improvement using the RCWA for crossed gratings," *J. Opt. Soc. Am. A*, Vol. 24, No. 9, 2880–2890, 2007.

6. Yang, H.-Y. D., R. Diaz, and N. G. Alexopoulos, "Reflection and transmission of waves from multilayer structures with planar-implanted periodic material blocks," *J. Opt. Soc. Am. B*, Vol. 14, No. 10, 2513–2521, Oct. 1997.

7. Shi, Y. and C. H. Chan, "Multilevel Green's function interpolation method for analysis of 3-D frequency selective structures using

volume/surface integral equation," *J. Opt. Soc. Am. A*, Vol. 27, No. 2, 308–318, 2010.

8. Van Beurden, M. C. and B. P. de Hon, "Electromagnetic modelling of antennas mounted on a band-gap slab — discretisation issues and domain and boundary integral equations," *Proc. of the Int. Conf. on Electromagnetics in Advanced Applications ICEAA'03*, R. D. Graglia (ed.), 637–640, Politecnico di Torino, Torino, 2003.

9. Chang, Y.-C., G. Li, H. Chu, and J. Opsal, "Efficient finite-element, Green's function approach for critical-dimension metrology of three-dimensional gratings on multilayer films," *J. Opt. Soc. Am. A*, Vol. 23, No. 3, 638–645, 2006.

10. Magath, T., "Coupled integral equations for diffraction by profiled, anisotropic, periodic structures," *IEEE Trans. Antennas Propag.*, Vol. 54, No. 2, 681–686, 2006.

11. Van Beurden, M. C., "Fast convergence with spectral volume integral equation for crossed block-shaped gratings with improved material interface conditions," *J. Opt. Soc. Am. A*, Vol. 28, No. 11, 2269–2278, 2011.

12. Kailath, T. and I. Koltracht, "Matrices with block Toeplitz inverses," *Linear Algebra Appl.*, Vol. 75, 145–153, 1986.

13. Götz, P., T. Schuster, K. Frenner, S. Rafler, and W. Osten, "Normal vector method for the RCWA with automated vector field generation," *Opt. Express*, Vol. 16, No. 22, 17295–17301, 2008.

14. Gohberg, I. and I. Koltracht, "Numerical solution of integral equations, fast algorithms and Krein-Sobolev equation," *Numer. Math.*, Vol. 47, 237–288, 1985.

15. Magath, T. and A. E. Serebryannikov, "Fast iterative, coupled-integral-equation technique for inhomogeneous profiled and periodic slabs," *J. Opt. Soc. Am. A*, Vol. 22, No. 11, 2405–2418, 2005.

16. Sleijpen, G. L. G. and D. R. Fokkema, "BiCGstab(ℓ) for linear equations involving unsymmetric matrices with complex spectrum," *Electron. Trans. Numer. Anal.*, Vol. 1, 11–32, 1993.

17. Johnson, S. G. and J. D. Joannopoulos, "Three-dimensionally periodic dielectric layered structure with omnidirectional photonic band gap," *Appl. Phys. Lett.*, Vol. 77, No. 22, 3490–3492, 2000.